HHS Public Access

Author manuscript

J Am Chem Soc. Author manuscript; available in PMC 2019 May 29.

Published in final edited form as:

J Am Chem Soc. 2017 April 05; 139(13): 4859–4865. doi:10.1021/jacs.7b00390.

Defect-Induced Near-Infrared Photoluminescence of Single-Walled Carbon Nanotubes Treated with Polyunsaturated Fatty Acids

Cheuk Fai Chiu[1], **Wissam A. Saidi**[2], **Valerian E. Kagan**[3], and **Alexander Star**[1,4,*]

[1]Department of Chemistry, University of Pittsburgh, Pittsburgh, Pennsylvania 15260, United States

[2]Mechanical Engineering and Materials Science, University of Pittsburgh, Pittsburgh, Pennsylvania 15260, United States

[3]Environmental and Occupational Health, University of Pittsburgh, Pittsburgh, Pennsylvania 15260, United States

[4]Bioengineering, University of Pittsburgh, Pittsburgh, Pennsylvania 15260, United States

Abstract

Single-walled carbon nanotubes (SWCNTs) have been incorporated in many emerging applications in the biomedical field including chemical sensing, biological imaging, drug delivery, and photothermal therapy. To overcome inherent hydrophobicity and improve their biocompatibility, pristine SWCNTs are often coated with surfactants, polymers, DNA, proteins, or lipids. In this paper, we report the effect of polyunsaturated fatty acids (PUFAs) on SWCNT photoluminescence. A decrease in the SWCNT bandgap emission (E_{11}) and a new red-shifted emission (E_{11}^{-}) were observed in the presence of PUFAs. We attribute the change in SWCNT photoluminescence to the formation of oxygen-containing defects by lipid hydroperoxides through photo-oxidation. The observed changes in near-infrared emission of SWCNTs are important for understanding the interaction between SWCNTs and lipid biocorona. Our results also indicate that photo-excited SWCNTs can catalyze lipid peroxidation similarly to lipoxygenases.

Graphical Abstract

*Corresponding Author astar@pitt.edu.

Supporting Information

Data for control experiments (S1-S12). This material is available free of charge via the Internet at http://pubs.acs.org

The authors declare no competing financial interests.

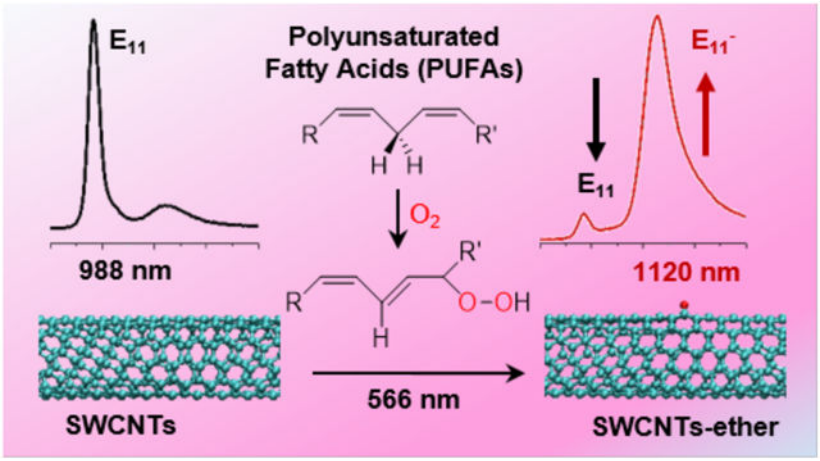

INTRODUCTION

Since its discovery in 2002, the bandgap luminescence of single-walled carbon nanotubes (SWCNTs) has been an important analytical tool for characterizing semiconducting SWCNTs.[1,2] SWCNT species of specific diameters and chiralities have distinct first (E_{11}), second (E_{22}), and third (E_{33}) excitonic transitions, allowing for their relative concentrations to be correlated from their emission intensities using an excitation-emission map (EE map).[2] The photoemission properties of SWCNTs have been investigated for applications in cancer diagnostics,[3,4] cell recognition,[4,5] and chemical sensing.[6,7] The bandgap luminescence is often quenched by the surrounding environment and chemical reactions,[8-10] in many cases, making SWCNTs a turn-off sensor thereby limiting its dynamic range.

A new SWCNTs emission band has been reported in recent years. Named E_{11}^-, or E_{11}*, this emission band has a turn-on mechanism that requires activation by a small degree of functionalization.[11-13] This “defect-induced” activation has been achieved by ozone,[11] diazonium,[12] alkycarboxylation,[13] hydrogen peroxide,[14] and other oxidants. Matsuda et al. compared the oxygen- and diazonium-based defects with respect to the E_{11}^- bands they produced. The researchers have concluded that the local electronic states generated from the defects are nearly independent of the origin.[15] Meanwhile, recent findings revealed that different functional groups on diazonium adducts could generate E_{11}^- peaks on (6,5) SWCNTs at a range of 1110 to 1148 nm.[12] For oxygen-based defects, Ghosh et al. deduced the product of their ozone-functionalized SWCNTs to be ethers perpendicular to nanotube axis (ether-perpendicular) rather than epoxides.[11] This ether-related E_{11}^- peak was reported at 1120 nm on a (6,5) SWCNT.[11] Ma et al. demonstrated that different oxygen functional groups on (6,5) SWCNTs could generate different emission peaks, with ether-perpendicular and epoxide causing peaks downshifted from the E_{11} band gap by ~135 (at 1115 nm) and 310 meV (at 1250 nm), respectively.[16] This E_{11}^- peak could be utilized in a turn-on sensor as opposed to the bandgap-based turn-off sensors. A recent utilization of this defect-induced peak was demonstrated by Wang and coworkers as a pH sensor and nano-thermometer.[17]

Lipids, especially those containing polyunsaturated fatty acids (PUFAs), can be oxidized to form lipid hydroperoxides.[18-21] The resulting peroxides can damage cell membranes,

resulting in cell death, and could be mutagenic and carcinogenic.[22] Enzymatic oxidation, by lipoxygenases, is also important in cell signaling.[23] We have previously functionalized SWCNTs with phospholipids, particularly phophatidylserine, to make them recognizable by different phagocytic cells.[24] We have also reported that SWCNTs selectively adsorbed two types of the most abundant surfactant phospholipids: phosphatidylcholines (PC) and phosphatidylglycerols (PG).[25]

In this work, we investigated photoluminescence (PL) emission of lipid-coated SWCNTs and observed the decrease in their E_{11} signal and formation of a new E_{11}^- emission under illumination conditions. In addition to PL spectroscopy, the nanotube samples were studied using Raman, X-ray photoelectron spectroscopy (XPS), diffuse reflectance infrared Fourier transform spectroscopy (DRIFTS), and density functional theory (DFT) calculations. Our results suggest that lipid hydroperoxides react with the sidewalls of SWCNTs and form oxygen-containing defects.

RESULTS

Figure 1 shows EE maps of (6,5) purified high-pressure carbon monoxide (HiPco) SWCNTs before and after reaction with linoleic acid (LA, C18:2) under illumination at 566 nm. A typical band gap luminescence from the (6,5) SWCNTs (E_{11}) was observed before the reaction (Figure 1a) and a new E_{11}^- peak, centered at ~1120 nm, dominated the EE map after the reaction (Figure 1b). Figure 1c shows the spectral changes during the reaction, revealing the decrease in the bandgap emission (E_{11}) and the increase in the defect-induced peak (E_{11}^-) over a reaction time of 60 mins. Figure 1d compares the UV-vis-NIR absorption of LA/SWCNTs with linoleic acid. Linoleic acid autoxidizes in air via a free radical chain reaction and forms linoleic acid hydroperoxide (LA-OOH), which gives a characteristic absorption at 235 nm due to the conjugated diene structure.[18-20] The shrinkage of this peak after reaction with SWCNTs indicates that LA-OOH was consumed in the process. The vis-NIR portion of the spectra also shows that bandgap absorptions of the SWCNTs, E_{11} and E_{22}, remain essentially unchanged after the reaction. The spectral changes in PL emission and UV-vis-NIR absorption are analogous to those observed during alkylcarboxylation and UV-ozone treatments.[11,13] The reaction between LA and SWCNTs was not specific to HiPco SWCNTs, as cobalt-molybdenum catalyzed (CoMoCAT) SWCNTs also provided similar results (Figure S1). Figure 1e shows the changes of emission intensity of E_{11} and E_{11}^- peaks of CoMoCAT SWCNTs over a reaction time of six hours. The E_{11} emission decreased in the first 30 minutes of the reaction, whereas the E_{11}^- intensity increased to a maximum after 60 mins and then subsequently decreased. The decline in the E_{11}^- peak was previously demonstrated by Wang and coworkers with diazonium functionalization.[12] The maximum emission at 1120 nm was reached by achieving optimal defect density on the SWCNTs, with further reaction resulting in over functionalization of SWCNTs with excess defects, and diminishing the E_{11}^- emission.

To ensure the effects were caused by the reaction between LA-OOH and SWCNTs, different control experiments were conducted. Figure S2a shows the spectral changes with LA and SWCNTs in the absence of surfactant. The E_{11}^- peak was still clearly observable after the reaction despite the low signal level due to the poor dispersibility of pristine SWCNTs.

SWCNT/sodium cholate (SC) produced a stable suspension with a non-photobleachable E_{11} photoluminescence, as documented in the literature,[6] and no evolvement of the E_{11}^- band (Figure S2b). Sodium cholate/linoleic acid did not produce any NIR emission signal, as there were no NIR emitters in the solution (Figure S2c). To demonstrate that linoleic acid hydroperoxide was responsible for functionalizing the SWCNTs, a sample of linoleic acid was pretreated with morin to inhibit the LA-OOH formation via terminating the radical chain reactions.[20] When SWCNTs were exposed to this pretreated linoleic acid, no enhancement in E_{11}^- emission was observed (Figure S2d). This is in agreement with our observation from Figure 1d, in which LA-OOH was consumed in the reaction process. From these control experiments, we conclude that the E_{11}^- peak was induced by photo-initiated reaction between LA-OOH and SWCNTs, and sodium cholate was merely acting as a surfactant, which improves the dispersibility of SWCNTs thus enhancing the emission signals.

The role of surfactant type and concentration were investigated and the results are summarized in Table 1. CoMoCAT SWCNTs were dispersed in sodium cholate (SC), sodium dodecyl sulfate (SDS) or sodium dodecylbenzene sulfonate (SDBS) at 0.1 wt. % and 1 wt. % surfactant concentrations, and reacted with linoleic acid. Emission spectra were collected before and after one hour of reaction time, and the changes of E_{11}^- intensities are reported in Table 1. Using SC or SDS at 0.1% concentration, the E_{11}^- peak formation is apparent (Figure S3). The reaction is slower at higher surfactant concentrations. Better shielding effect is expected at higher concentrations, as the increase in surfactant density provided better coverage of nanotube surface, suggesting that the photochemical reaction between LA-OOH and SWCNTs was a surface event. Interestingly, the E_{11}^- formation reaction is inefficient when SDBS was used.

We investigated the effect of illumination wavelength on reaction efficiency as shown in Figure 2a. The emission spectra were analyzed using 566 nm wavelength before and after illumination at various wavelengths (235, 366, 466, 566, and 666 nm) for 60 minutes. The apparent quantum efficiency (AQE) was calculated using the changes of the defect-induced (E_{11}^-) emission peaks corrected by the photon flux of the wavelength used.[26] The resulting AQE values were normalized to the highest value for simplicity. All values are available in Table S1. We observed the highest efficiency with 566 nm illumination, the wavelength which matches the absorption (E_{22} transition) band of (6,5) SWCNTs. This result suggests that the mechanism of the reaction involves the excited state of the SWCNTs, but not the excited state of lipid hydroperoxide as demonstrated by the lack of E_{11}^- formation at 235 nm excitation.

To further investigate the photochemical nature of the reaction between LA and SWCNTs, the samples were stored in the dark for three days, before being illuminated with 566 nm light for 1 hour (Figure 2b). When the samples were stored in the dark, no evolvement of the E_{11}^- peak was observed. The same solutions were subsequently activated by excitation with 566 nm light, showing E_{11}^- progression dependent on LA-OOH concentration. From our data, we calculated the minimum ratio required is ~5 nmol of LA-OOH : 0.01 mg of SWCNTs. At lower ratios, the spectral difference was not significant. We expect this ratio is

efficient for in vivo detection of lipid hydroperoxide, though this is beyond the scope of this paper.

The observed results are comparable to other defect-induced luminescence examples reported in the literature.[11-13] In all cases, the new E_{11}^- peaks were attributed to defects on the SWCNT sidewalls. Nanotube defect formation was confirmed by Raman spectroscopy. Figure 3a shows the Raman spectra of SWCNTs with an increase of D/G ratio from 0.13 to 0.27 after the reaction, indicating a slight increase in defect density.

SWCNT samples were further analyzed using XPS and DRIFTS. Figure 3b shows low-resolution, or survey, XPS spectra and the high-resolution spectra of the oxygen peak. From the survey spectra, it is clear that SWCNTs were oxidized upon LA reaction as illustrated by the increase of the carbon:oxygen ratio from 1.00:0.10 to 1.00:0.32. High-resolution peaks were deconvoluted and showed an increase in C—O (~532 eV) in comparison to C═O (~531 eV) in the oxygen spectra (Figure 3c).[27-29] The increase of C—O bonding is also observed in the carbon spectra (Figure S4) and can be attributed to hydroxyl or ether bonds.[16,29]

Figure 3d shows the DRIFTS spectra of LA/SWCNTs with and without light activation. The two samples showed similar intensities in hydroxyl (O—H) and alkyl (C—H) bonding. The major difference is at 1000-1200 cm^{-1}, attributed to ether (C—O—C) or hydroxyl (O—H) bonds.[30,31] However, the hydroxyl band does not change significantly in the ~3400 cm^{-1} region, implying that the density of O—H groups do not increase on the CNT surface. Therefore, assignment of the ~1100 cm^{-1} band to ether or epoxide group (C—O—C) is more dependable.

We further investigated the electronic structure of oxidized (6,5) SWCNTs using DFT calculations by examining different oxidizing agents namely, O, O_2 and O_3. For the oxygen-doped CNT, we find that the most favorable adsorption configuration is at the bridge site on a carbon bond that is nearly perpendicular to the tube axis. In this configuration, the C-C bond at which oxygen is adsorbed increases to 2.08 Angstrom from its original length of 1.43 Angstrom for the undoped CNT. Further, the C-O bond is nearly 1.39 Angstrom. We will refer to this configuration as ether-perpendicular. The second most favorable adsorption site is the bridge site that is parallel to the tube axis with a binding energy that is nearly 1eV higher than ether-perpendicular. We will refer to this configuration as epoxide-parallel as oxygen with the two carbon atoms that it bonds to form nearly an equilateral triangle (C-C bond is 1.52 Angstrom, and C-O bond is 1.46 Angstrom). These results are consistent with references.[11,16] For O_2-doped CNT, we find that energetically it is nearly the same whether O_2 bonds to the two carbon atoms that are nearly parallel or perpendicular to the CNT tube axis. For O_3-doped CNT, we find that the ozone molecule can be stabilized only by bonding to C-C that is perpendicular to the tube axis.

The oxidation of the CNTs introduces new adsorption bands as can be seen from Table 2 and Figure S5. For ether-perpendicular configuration, the new absorption band E_{11}^- is located nearly ~200 meV lower in energy than that of the bright exciton E_{11} band of the pristine CNT. This is consistent with the results of Ma et al. where this model was investigated using

B3LYP.[16] In our calculations, we noticed that the exciton peaks at the B3LYP level are lower in energy than those at the CAM-B3LYP level.

The functionalization reaction between SWCNTs and linoleic acid reported here can also be observed with other PUFAs and lipids. Figure S6 and S7 show the spectral changes of SWCNTs with γ-linolenic acid (18:3) and cardiolipin (18:2). The decrease in E_{11} and increase in E_{11}^- were observed in both cases. Saturated stearic acid (18:0) and stearoyl-cardiolipin (14:0), on the other hand, did not produce any spectral changes. These results demonstrated that the reaction reported here require unsaturated fatty acids/lipids, and cannot be repeated with saturated ones. This is in agreement with our proposed mechanism that reaction undergoes the formation of lipid hydroperoxides.

DISCUSSION

Scheme 1 summarizes the photochemical reaction between SWCNT and linoleic acid reported in this work. Linoleic acid autoxidizes through radical chain reactions to form linoleic acid hydroperoxide.[18-20] The linoleic acid hydroperoxide further reacts with photo-excited SWCNTs, forming ether defects on the nanotube surface.

The autoxidation of PUFAs is well documented in the literature, and involves radical chain reaction to produce lipid hydroperoxide with conjugated diene structure.[18-20] Our UV-vis-NIR absorption spectra reveal the characteristic 235 nm peak of lipid hydroperoxides and its reduction upon reaction with SWCNTs (Figure 1d). Using morin as an antioxidant to terminate the radical chain reaction,[19,20] we have further demonstrated (Figure S2d) that the restricted formation of lipid hydroperoxide could limit the SWCNTs functionalization.

The photoreaction between linoleic acid hydroperoxide and SWCNTs is expected to take place on the nanotube surface as demonstrated by experiments with different surfactants (Table 1). The hydrophobic ends of fatty acids can interact with the hydrophobic surface of the SWCNTs in a way similar to SDS. At higher surfactant concentrations, the SWCNTs are better protected by higher surfactant density and hence E_{11}^- formations were less profound. Moreover, we speculate that the different result for SDS and SDBS was due to the different SWCNT surface coverage, in which SDBS arranged parallel to the nanotube surface to maximize π-π stacking and provided better shielding from oxidation.

Lipid hydroperoxides can be decomposed into peroxyl radicals and alkoxyl radicals.[32] The decomposition of lipid hydroperoxides can be catalyzed by transition metals, which pristine SWCNTs contain as residual catalysts from nanotube synthesis. The fact that reaction can undergo with both CoMoCAT and HiPco SWCNTs suggests that metal catalyst should not be the factor, as the two SWCNTs contain different metals but give similar results. We further dismiss the effect of metal ions by adding diethylenetriaminepentaacetic acid (DTPA) to the reaction as a metal chelator (Figure S8).[33] E_{11}^- emission from LA/SWCNTs was detected in the presence of DTPA, suggesting that the effect of metal is minimal. It is possible that excitons on SWCNTs are catalyzing the decomposition of lipid hydroperoxides like free electrons in metal. A similar argument was proposed by Wang and coworkers, in which the oxidation potential of SWCNTs was raised by the excited electrons.[26] Such

pathway might produce radicals that functionalized SWCNTs regardless of the presence of metal. To test this hypothesis, antioxidants were added to SWCNTs before subjected to linoleic acid hydroperoxide. In the presence of antioxidants, the E_{11}^- emission from SWCNTs was not observed, suggesting that the functionalization reaction might undergo via radical formation (Figure S9). Upon reaction, the linoleic acid hydroperoxide is expected to be reduced to form hydroxylated linoleic acid and other associated products, including 2-hydroxyheptanal and 4-hydroxy-2-nonenal (HNE).[19,34,35] The results suggest that lipid peroxidation process, typically catalyzed in vivo by iron-containing enzymes and monitored using chemiluminescence schemes, can be facilitated by SWCNTs, where their NIR fluorescence can be used to study the lipid peroxidation.

In principle, the oxidation of SWCNTs by LA-OOH could result in an addition of oxygen functional groups on the nanotubes (e.g., hydroxyl, ether and epoxide) or the covalent grafting of fatty acid to SWCNTs through ether bonding (SWCNT—O—LA). The attachment of linoleic acid to SWCNT should generate a carboxyl signal in the HRXPS at ~534 eV in oxygen band,[27] and ~289 eV in the carbon band.[28] The absence of these peaks suggests that the attachment of linoleic acid to SWCNTs is unlikely. Similar conclusions can be drawn from the DRIFTS spectra. The signature O-H bonds (3400 cm^{-1}) and carbonyl bonds (1700 cm^{-1}) from carboxyl groups were not detected. Instead, an increase at 1000-1300 cm^{-1} from C—O bonds was observed. Although there is a small peak at 2968 cm^{-1} and moderate ones at 1262 and 805 cm^{-1}, and can all be assigned to C—H bonding, their changes were relatively small compared to the C-O bonding.

Although HRXPS and DRIFTS can refute the grafting of linoleic acid on CNT surface, these techniques do not directly reveal the chemical identity of the functional groups. The observed increase in C-O bonding can be related to different oxygen-containing functional groups. In determining the origin of these induced defects, we compared the observed E_{11}^- peak with values calculated by DFT and previously reported by Ma et al.[16] Our E_{11}^- peak, downshifted by 130 meV from the E_{11} bandgap, matches closely with the calculated and previously reported value for ether-perpendicular. This is also in agreement with earlier work by Ghosh et al., who associated ether functional groups perpendicular to the tube axis with their observed E_{11}^- emission from ozonation.[11] In our work, a radical reaction might involve the addition of OH or fatty acid, yet neither of them was detected in our characterization. The formation of epoxide should generate a defect-induced peak at ~1250 nm in the emission spectrum, which was not detected in this work.[16] Based on the position of the E_{11}^- peak at 1120 nm, assigning the functional group to ether is more dependable.[16] The assignment of this defect-induced band to ether groups might also explain the low emission intensity at 1120 nm before the reaction. It was shown in the literature that as-produced SWCNTs contain defects,[36] some of which are oxygen moieties.[37] A noticeable C-O bonding in the oxygen HRXPS from our starting SWCNTs could be evidence of a small amount of ether defects.

Our data from Figure 2 have shown that the reaction is photochemical. Additional experiments were conducted to show that reaction can be stopped and product harvested for doping purposes. SWCNTs/LA-OOH reaction can be ceased by removing the sample from light. A reacted sample was withdrawn from the illumination and stored in the dark for

seven days, and resembled similar spectral features before and after storage (Figure S10a,b). To illustrate the isolation of reacted SWCNTs, another sample was treated with LA-OOH (Figure S10c), dialyzed overnight to remove surfactants and linoleic acid. The isolated SWCNTs were redispersed in bovine serum albumin and showed a similar emission profile before and after the isolation (Figure S10d).

Although our data indicate that the reaction has a higher efficiency when excited at a wavelength in resonance with the SWCNT bandgap, the reaction can be initiated using white light. SWCNTs were sonicated with linoleic acid under normal laboratory lighting condition, and the development of E_{11}^- band was observed (Figure S11). The finding here is important when considering SWCNT-unsaturated fatty acid/liposome complexes prepared in the lab.[38] We recommend that SWCNT-liposome complex be prepared in the dark and oxygen-free environment to prevent undesired CNT oxidation. While all our data point to a photochemical reaction, we cannot rule out the possibility that the PUFA-SWCNTs reaction can undergo without light at an extremely slow rate, and was only made possible to detect by excitation enhancement. As recently demonstrated by Wang et al. reaction rate between SWCNTs and diazonium salts were enhanced by resonant light at nanotube E_{22}, E_{33}, and E_{44} transitions.[26] Such effect at E_{33} transition was not observed in our work. We attribute this to the low absorbance at E_{33} in our sample and the insufficient excitation at this wavelength due to low power density.

CONCLUSION

We demonstrate that PUFAs can oxidize SWCNTs under ambient conditions. We attribute this new reaction to the autoxidation of PUFAs capable of forming lipid hydroperoxides resulting in the formation of ether functional groups on the sidewall of SWCNTs. The reaction is photochemical and is more efficient when the illuminating light matches the resonance wavelength of the nanotubes. More importantly, the functionalization dramatically changes the optical and electronic properties of the SWCNTs, resulting in a new E_{11}^- band emission. Our data also suggests that the photoexcited nanotube surface might be catalyzing the decomposition of lipid hydroperoxide. These findings, in addition to providing a new understanding of SWCNT-lipid interactions, can be potentially used for in vivo lipid peroxidation detection.

MATERIALS AND METHODS

Linoleic acid (Sigma L1376) was autoxidized in air. The concentration of lipid hydroperoxide produced was determined by UV-vis absorption at 235 nm at which the linoleic acid hydroperoxide (LA-OOH) has a molar attenuation coefficient of 25000 L mol^{-1} cm^{-1}.[18,23] Morin and ascorbic acid were purchased from Sigma-Aldrich.

Purified high-pressure carbon monoxide (HiPco) produced SWCNTs with (6,5) chirality was obtained from Atom Nanoelectronic. Cobalt-molybdenum catalyzed (CoMoCAT) single-walled (6,5) carbon nanotubes were purchased from Sigma-Aldrich. SWCNT suspension was prepared at 0.02 mg/mL concentration with 0.1 wt. % sodium cholate ((SC); Sigma-Aldrich) as a surfactant unless otherwise stated. The HiPco SWCNTs stock solution

was dispersed in 2 wt. % mixture of SC and SDS and was diluted ten times before used. The suspension was sonicated for 1 hour and centrifuged to remove large bundles. The top 90% of the supernatant was transferred to a separate container and used as stock. Sodium dodecyl sulfate (SDS) and sodium dodecylbenzene sulfonate (SDBS) were purchased from Sigma-Aldrich and used without further purification. The SWCNT supernatant (500 μL) was exposed to 1.4~140 μM of linoleic acid hydroperoxide. Samples were illuminated with 566 nm light for 60 minutes unless stated otherwise. Emission spectra were obtained every 5 minutes during this period. Excitation-emission maps (EE maps) and absorption spectra were obtained both before and after the reaction.

Photoluminescence measurements were obtained using a Nanolog spectrofluorometer (HORIBA Jobin Yvon) equipped with a xenon lamp (400 W) light source, double excitation monochromators, and Symphony II InGaAs array (NIR) detector. For the EE maps, the excitation wavelength was scanned from 300 to 800 nm in 5 nm increments, and the emission was detected between 820 nm to 1580 nm with 1.5 nm increments. Spectra were obtained using 566 nm excitation wavelength, which is in resonance with the second absorption band of the (6,5) SWCNTs. Slit widths were set at 10 nm for both excitation and emission. All measurements were obtained with an 830 nm longpass filter at ambient temperature. Power density was measured independently with an optical power meter (Thorlabs PM200) and detector (Thorlabs S120VC). The power density at 566 nm was 7.49 mW/cm^2. Power densities at other wavelengths are available in the Table S1.

UV–vis–NIR measurements were acquired using a PerkinElmer Lambda 900 spectrophotometer over the wavelength range of 200–1200 nm.

Raman measurements were performed using a XploRA plus Raman microscope with a 532 nm laser (HORIBA). SWCNTs were drop-cast on a glass slide and allowed to dry under ambient conditions overnight, thereby forming aggregates of SWCNTs. Scans were carried out at a laser power of 2.5 mW with an accumulation time of 15 s over the range from 200 to 3200 cm^{-1}. Spectra were acquired from multiple locations, and the results were normalized to the most intense peak. D/G ratios were calculated by integrating the area under the peaks.

X-ray photoelectron spectroscopy (XPS) was performed on a Thermo Scientific K-Alpha using monochromated Al Kα X-rays as the source. SWCNTs were reacted with LA-OOH for ~6 hr to increase the defect density for a better signal response. Samples were collected from multiple runs to obtain the amount required for XPS analysis. The SWCNT samples were dialyzed with 1kD membrane (Spectra/Por 7 MWCO) for three days to remove the surfactant and linoleic acid. The aggregated SWCNTs were collected in water and solvent-extracted using ethyl acetate. Samples in ethyl acetate were drop-cast on a glass slide and dried at 60 °C in vacuum for 6 hours prior to measurements.

Diffuse-reflectance Infrared Fourier transform spectroscopy (DRIFTS) was performed employing an IR-Prestige spectrophotometer (Shimadzu Scientific) outfitted with an EasiDiff accessory (Pike Technologies). Samples were mixed with KBr and vacuum-dried for 3 hours prior to measurement. Spectra were averaged from 160 scans per sample over the

range of 500 to 4000 cm^{-1} with a resolution of 2 cm^{-1}. Kubelka-Munk conversion was applied.

DFT calculations were performed using FHI-aims[39] and Gaussian 09 program[40]. The (6,5) CNT was modeled using a cluster model with one repeat unit of the primitive unitcell with 386 atoms, amounting to a tube segment with a length of ~40 Angstrom. The carbon atoms at both ends were replaced with hydrogen to eliminate the dangling bonds and any spurious end-effects such as having edge-states. This approach has been applied in several studies.[16,41-43] The CNT oxidation was carried out using atomic oxygen, O_2, and O_3 where the functionalization is done in the middle of the group to avoid spurious edge state effects. The optimum structures of the CNTs were obtained by relaxing the atomic position of all atoms using a convergence threshold of 0.01 eV/Angstrom. For this, we used PBE as implemented in FHI-aims using a tier-1 basis set. Using the optimum structures, the excited states and the absorption spectra of the pristine and functionalized CNTs were investigated CAM-BLYP functional.[44] The CAM-B3LYP is a hybrid long-range order corrected functional, which in particular improves the description of charge transfer states. For comparison with previous study by Ma et al.,[16] we also computed the absorption spectra profile using B3LYP. All of our calculations were done using STO-3G consistent with previous studies.

Supplementary Material

Refer to Web version on PubMed Central for supplementary material.

ACKNOWLEDGMENT

The project described herein was supported by the National Institute of Environmental Health Sciences (Award R01ES019304).

REFERENCES

(1). O'Connell MJ; Bachilo SM; Huffman CB; Moore VC; Strano MS; Haroz EH; Rialon KL; Boul PJ; Noon WH; Kittrell C; Ma J; Hauge RH; Weisman RB; Smalley RE Science 2002, 297, 593–596. [PubMed: 12142535]

(2). Bachilo SM; Strano MS; Kittrell C; Hauge RH; Smalley RE; Weisman RB Science 2002, 298, 2361–2366. [PubMed: 12459549]

(3). Robinson JT; Welsher K; Tabakman SM; Sherlock SP; Wang H; Luong R; Dai H Nano Res. 2010, 3, 779–793. [PubMed: 21804931]

(4). Welsher K; Liu Z; Sherlock SP; Robinson JT; Chen Z; Daranciang D; Dai H Nat. Nanotechnol. 2009, 4, 773–780. [PubMed: 19893526]

(5). Welsher K; Liu Z; Daranciang D; Dai H Nano Lett. 2008, 8, 586–590. [PubMed: 18197719]

(6). Barone PW; Baik S; Heller DA; Strano MS Nat. Mater. 2004, 4, 86–92. [PubMed: 15592477]

(7). Kruss S; Landry MP; Ende E. Vander; Lima BMA; Nigel F; Zhang J; Nelson J; Mu B; Hilmer A; Strano M; Vander Ende E; Lima BMA; Reuel NF; Zhang J; Nelson J; Mu B; Hilmer A; Strano M J. Am. Chem. Soc. 2014, 136, 713–724. [PubMed: 24354436]

(8). Jain A; Homayoun A; Bannister CW; Yum K Biotechnol. J. 2015, 10, 447–459. [PubMed: 25676253]

(9). Hong G; Diao S; Antaris AL; Dai H Chem. Rev. 2015, 115, 10816–10906. [PubMed: 25997028]

(10). Iverson NM; Barone PW; Shandell M; Trudel LJ; Sen S; Sen F; Ivanov V; Atolia E; Farias E; McNicholas TP; Reuel N; Parry NMA; Wogan GN; Strano MS Nat. Nanotechnol. 2013, 8, 873–880. [PubMed: 24185942]

(11). Ghosh S; Bachilo SM; Simonette R. a; Beckingham KM; Weisman RB Science 2010, 330, 1656–1659. [PubMed: 21109631]

(12). Piao Y; Meany B; Powell LR; Valley N; Kwon H; Schatz GC; Wang Y Nat. Chem. 2013, 5, 840–845. [PubMed: 24056340]

(13). Zhang Y; Valley N; Brozena AH; Piao Y; Song X; Schatz GC; Wang YJ. Phys. Chem. Lett. 2013, 4, 826–830. [PubMed: 26281939]

(14). McDonald TJ; Blackburn JL; Metzger WK; Rumbles G; Heben MJ J. Phys. Chem. C 2007, 111, 17894–17900.

(15). Ohno Y; Maruyama S; Takashi M; Iwamura M; Akizuki N; Miyauchi Y; Mouri S; Shaver J; Gao Z; Cognet L; Lounis B; Matsuda K ACS Nano 2014, 8, 11254–11260. [PubMed: 25331628]

(16). Ma X; Adamska L; Yamaguchi H; Yalcin SE; Tretiak S; Doorn SK; Htoon H ACS Nano 2014, 8, 10782–10789. [PubMed: 25265272]

(17). Kwon H; Kim M; Meany B; Piao Y; Powell LR; Wang YJ. Phys. Chem. C 2015, 119, 3733–3739.

(18). Jussila M; Sundberg S; Hopia A; Mäkinen M; Riekkola ML Electrophoresis 1999, 20, 111–117. [PubMed: 10065966]

(19). Wanasundara PKJPD; Shahidi F In Bailey's Industrial Oil and Fat Products; John Wiley & Sons, Inc.: Hoboken, NJ, USA, 2005.

(20). Torel J; Cillard J; Cillard P Phytochemistry 1986, 25, 383–385.

(21). Wisastra R; Dekker FJ Cancers (Basel). 2014, 6, 1500–1521. [PubMed: 25037020]

(22). Marnett LJ Mutat. Res. 1999, 424, 83–95. [PubMed: 10064852]

(23). Vick BA; Zimmerman DC Plant Physiol. 1987, 85, 1073–1078. [PubMed: 16665806]

(24). Konduru NV; Tyurina YY; Feng W; Basova LV; Belikova NA; Bayir H; Clark K; Rubin M; Stolz D; Vallhov H; Scheynius A; Witasp E; Fadeel B; Kichambare PD; Star A; Kisin ER; Murray AR; Shvedova AA; Kagan VE PLoS One 2009, 4, e4398. [PubMed: 19198650]

(25). Kapralov AA; Feng WH; Amoscato AA; Yanamala N; Balasubramanian K; Winnica DE; Kisin ER; Kotchey GP; Gou P; Sparvero LJ; Ray P; Mallampalli RK; Klein-Seetharaman J; Fadeel B; Star A; Shvedova AA; Kagan VE ACS Nano 2012, 6, 4147–4156. [PubMed: 22463369]

(26). Powell LR; Piao Y; Wang YJ. Phys. Chem. Lett. 2016, 7, 3690–3694. [PubMed: 27588432]

(27). Arrigo R; Hävecker M; Wrabetz S; Blume R; Lerch M; McGregor J; Parrott EPJ; Zeitler JA; Gladden LF; Knop-Gericke A; Schlögl R; Su DS J. Am. Chem. Soc. 2010, 132, 9616–9630. [PubMed: 20583786]

(28). Tien HW; Huang YL; Yang SY; Wang JY; Ma CCM Carbon 2011, 49, 1550–1560.

(29). Zhang W; Zhang H; Xiao J; Zhao Z; Yu M; Li Z Green Chem. 2014, 16, 211–220.

(30). Barros EB; Filho AGS; Lemos V; Filho JM; Fagan SB; Herbst MH; Rosolen JM; Luengo CA; Huber JG Carbon 2005, 43, 2495–2500.

(31). Jiang T; Xu K; Ji S J. Chem. Soc. Faraday Trans. 1996, 92, 3401.

(32). Gardner HW Free Radic. Biol. Med. 1989, 7, 65–86. [PubMed: 2666279]

(33). Llobet JM; Domingo JL; Corbella J Arch. Toxicol. 1986, 58, 278–281. [PubMed: 3087329]

(34). Loidl-Stahlhofen A; Hannemann K; Spiteller G Biochim. Biophys. Acta - Lipids Lipid Metab. 1994, 1213, 140–148.

(35). Wilcox AL; Marnett LJ Chem. Res. Toxicol. 1993, 6, 413–416. [PubMed: 8374035]

(36). Cherukuri TK; Tsyboulski DA; Weisman RB ACS Nano 2012, 6, 843–850. [PubMed: 22128755]

(37). Dementev N; Feng X; Borguet E Langmuir 2009, 25, 7573–7577. [PubMed: 19563231]

(38). Tunuguntla RH; Allen FI; Kim K; Belliveau A; Noy A Nat. Nanotechnol. 2016, 11, 639–644. [PubMed: 27043198]

(39). Blum V; Gehrke R; Hanke F; Havu P; Havu V; Ren X; Reuter K; Scheffler M Comput. Phys. Commun. 2009, 180, 2175–2196.

(40). Frisch MJ; Trucks GW; Schlegel HB; Scuseria GE; Robb MA; Cheeseman JR; Scalmani G; Barone V; Mennucci B; Petersson GA; Nakatsuji H; Caricato M; Li X; Hratchian HP; Izmaylov AF; Bloino J; Zheng G; Sonnenberg JL; Hada M; Ehara M; Toyota K; Fukuda R; Hasegawa J; Ishida M; Nakajima T; Honda Y; Kitao O; Nakai H; Vreven T; Montgomery JA Jr.; Peralta JE;

Ogliaro F; Bearpark MJ; Heyd J; Brothers EN; Kudin KN; Staroverov VN; Kobayashi R; Normand J; Raghavachari K; Rendell AP; Burant JC; Iyengar SS; Tomasi J; Cossi M; Rega N; Millam NJ; Klene M; Knox JE; Cross JB; Bakken V; Adamo C; Jaramillo J; Gomperts R; Stratmann RE; Yazyev O; Austin AJ; Cammi R; Pomelli C; Ochterski JW; Martin RL; Morokuma K; Zakrzewski VG; Voth GA; Salvador P; Dannenberg JJ; Dapprich S; Daniels AD; Farkas Ö; Foresman JB; Ortiz JV; Cioslowski J; Fox DJ Gaussian 09, 2009.

(41). Tretiak S Nano Lett. 2007, 7, 2201–2206. [PubMed: 17497817]

(42). Saidi WA; Norman P Phys. Chem. Chem. Phys. 2014, 16, 1479–1486. [PubMed: 24301905]

(43). Saidi WA; Norman P Carbon 2014, 67, 17–26.

(44). Yanai T; Tew DP; Handy NC Chem. Phys. Lett. 2004, 393, 51–57.

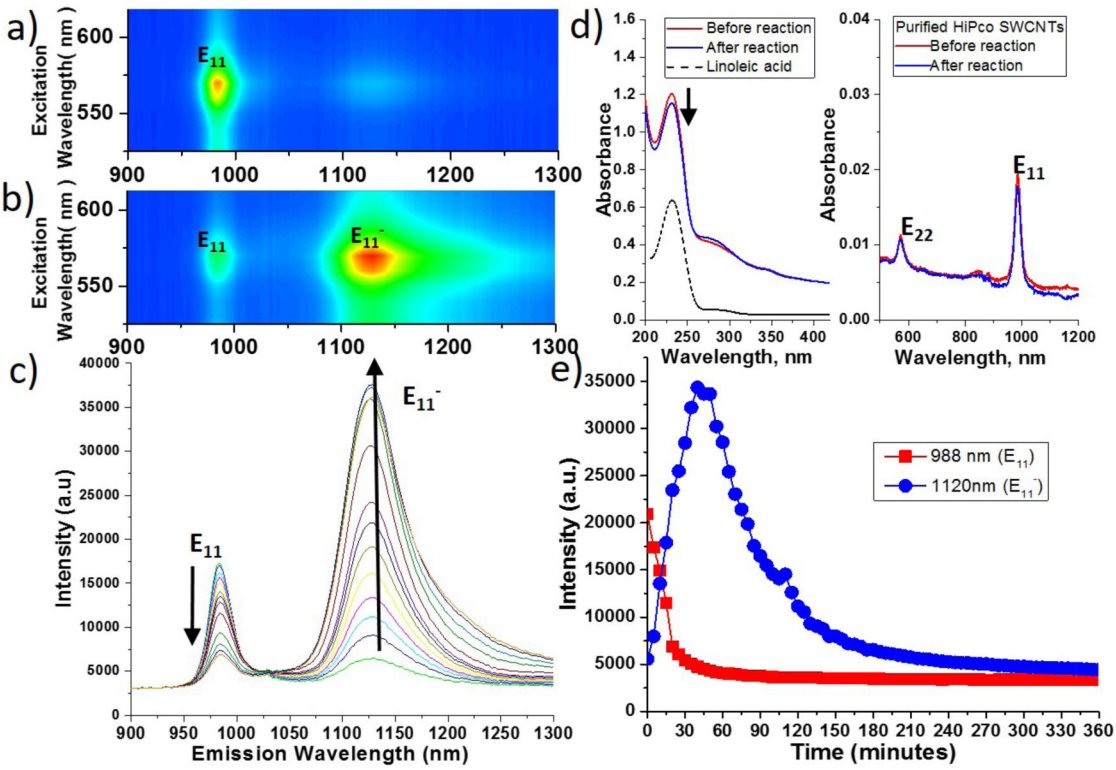

Figure 1.

EE maps of (6,5) purified HiPco SWCNTs a) before and b) after reaction with linoleic acid. Panel c) shows the spectral changes over 60 mins (spectra taken every 5 mins). d) UV-Vis absorption spectra showing the presence of lipid hydroperoxide (235 nm) and its concentration decreasing after reaction with SWCNTs. SWCNTs vis-NIR absorptions were un-shifted. e) Emission intensities of E_{11}^{-} and E_{11} of CoMoCAT SWCNTs reacted with linoleic acid over 6 hours.

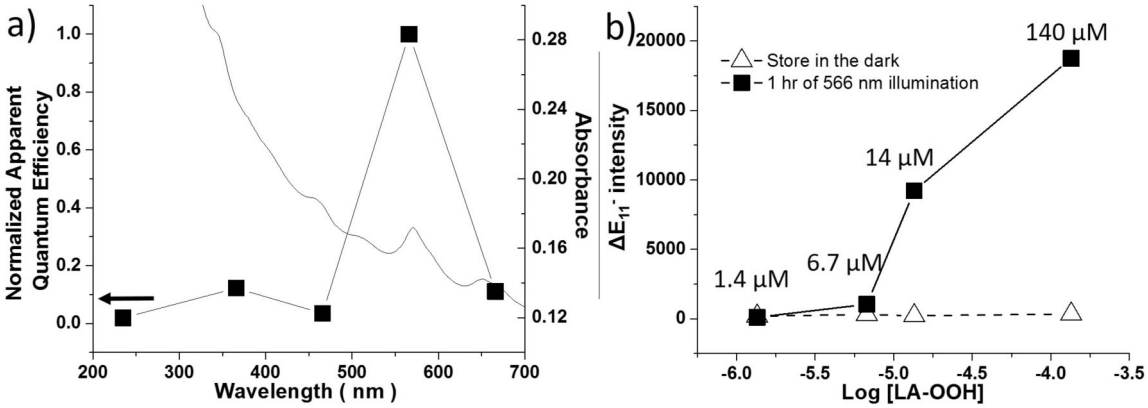

Figure 2.

a) Normalized apparent quantum efficiency of the reaction illuminated at different wavelengths (235, 366, 466, 566, 666 nm). All data points were collected with 566 nm excitation and efficiency was corrected to photon flux. UV-vis absorption of SWCNTs suspension is shown on the right axis. b) The effect of LA-OOH concentration on the SWCNT NIR emission. Samples were stored in the dark for 3 days, then activated with 566 nm illumination for 1 hour.

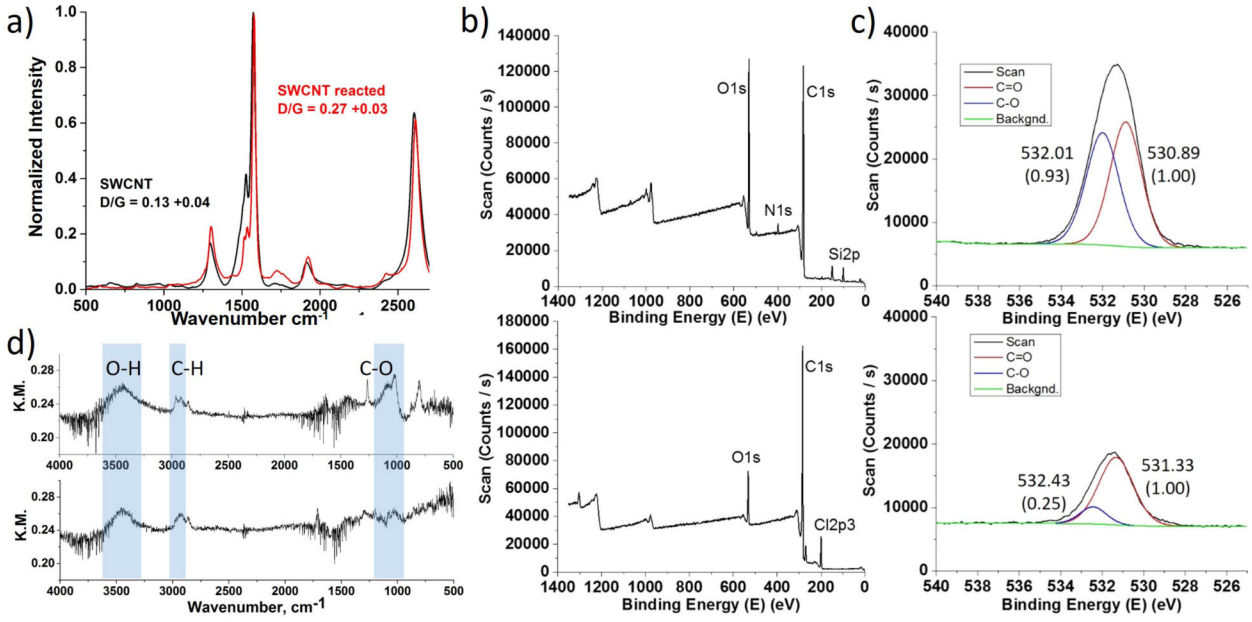

Figure 3.

a) Raman, b) XPS survey and c) the high-resolution spectra of the oxygen peak, and d) DRIFTS spectra of LA-OOH/SWCNTs after (top) and before (bottom) illumination.

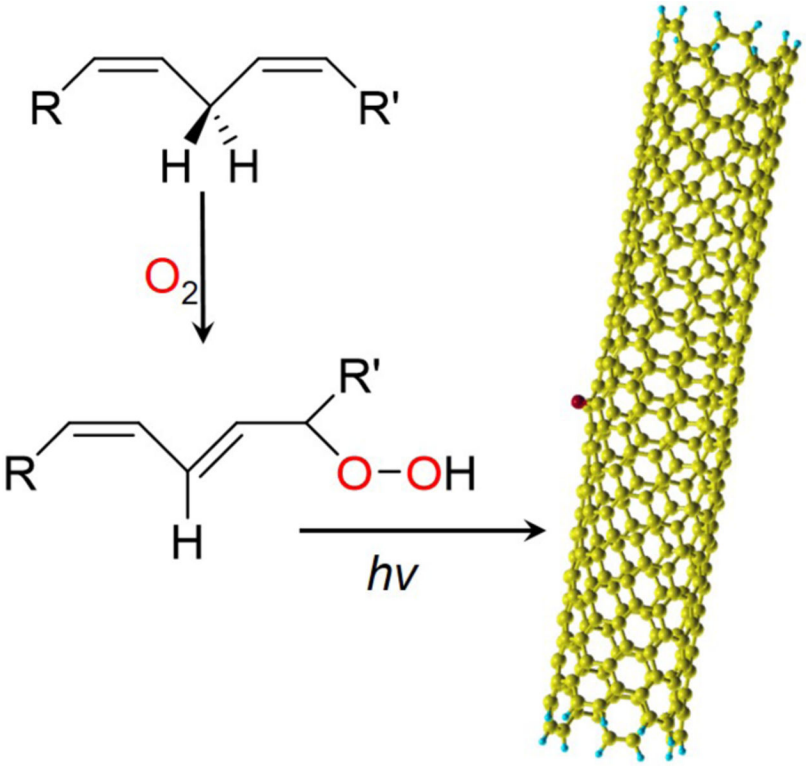

Scheme 1.
The proposed reaction between polyunsaturated fatty acids/lipids and SWCNTs.

Table 1.

Reaction progression (ΔE_{11}^{-} intensity) with different surfactants at two concentrations *

Surfactant	Concentration	
	0.1 %	**1.0 %**
Sodium cholate (SC)	14975	−160
Sodium dodecyl sulfate (SDS)	15506	578
Sodium dodecylbenzene sulfonate (SDBS)	1015	−257

* $\Delta E_{11}^{-} = (E_{11}^{-})_{final} - (E_{11}^{-})_{initial}$

Table 2.

Computation of electronic properties of undoped and oxygen-doped (6,5) SWCNTs

	Exciton peak (eV)	Shifts (eV)
Pristine CNT	2.180	-
Ether-perpendicular	2.000	−0.180
Epoxide-parallel	1.696	−0.484
O_2-parallel	1.906	−0.274
O_2-perpendicular	1.557	−0.622
O_3-perpendicular	1.877	−0.303